Supporting Information

Engineering Metallic MoS_2 Monolayers with Responsive Hydrogen Evolution Electrocatalytic Activities for Enzymatic Reaction Monitoring

Bang Lin Li, Cheng-Bin Gong, Wei Shen, Jing-Dong Peng, Hao Lin Zou, Hong Qun Luo* and Nian Bing Li**

Laboratory of Luminescence Analysis and Molecular Sensing (Southwest University), Ministry of Education, School of Chemistry and Chemical Engineering, Southwest University, Chongqing 400715, P. R. China.

*Correspondence and requests for materials should be addressed to B. L. Li (chemlibl@swu.edu.cn), H. Q. Luo (luohq@swu.edu.cn) and N. B. Li (linb@swu.edu.cn).

1. Experimental Procedures

1.1. Materials

Molybdenum disulfide (MoS_2 crystalline powder, < 2 μm, 99%) was obtained from Sigma-Aldrich Co. (USA). Glucose oxidase (GOD, BC grade) was purchased from Sangon Biotech (Shanghai) Co., Ltd. Sodium cholate (98%), glucose, disodium hydrogen phosphate, and sodium dihydrogen phosphate were obtained from Aladdin Chemistry Co. Ltd. (Shanghai, China). N-butyllithium (n-BuLi, 2.5 mol/L) was obtained from Adamas Reagent, Ltd (Shanghai, China). Other chemicals were of analytical reagent grade and used without further purification. Ultrapure water (18.2 MΩ/cm) was utilized throughout the whole experiment. The carbon paper substrates were purchased from Toray Industries Co. (Japan).

1.2. Experimental Instrumentations

The apparatuses of Schlenk line for "one-pot" chemical exfoliation of MoS_2 were purchased from Tansoole Co. Ltd. (Shanghai, China). A KQ-400B ultrasonic bath (400 W, Kunshan Ultrasonic Instruments Co., Ltd., China) was adopted for the liquid-phase exfoliation of MoS_2 crystals. The absorption spectra were recorded on a UV-2450 UV-vis spectrophotomer (Shimadzu, Japan). The defects and crystal lattices characterizations were conducted using a Tecnai G2 T20 UTWIN (FEI, USA) transmission electron microscope (TEM). The morphologies of MoS_2 before and after the exfoliation were observed from the Regulus 8100 (Hitachi, Japan) scanning electron microscope (SEM). The thicknesses of layered MoS_2 were measured by atomic force microscope (AFM, Multi-Mode, Bruker). X-ray photoelectron spectra (XPS) results were analyzed using an ESCALAB 250Xi X-ray photoelectron spectroscope (Thermo Electron, USA). Electrochemical measurements were conducted on the CH660E electrochemical workstation (Chenhua, China). Inductively coupled plasma-mass spectra (ICP-MS) were employed for the quantitative analysis of Mo species concentrations (Agilent 7800ce, USA).

1.3. Liquid-Exfoliation of MoS_2

Briefly, a portion of 100.0 mL mixed aqueous dispersion, containing 5.0 mg/mL MoS_2 powders and 1.5 mg/mL sodium cholate, was treated with sonication (25℃, 20 h). The resultant dispersion was centrifuged (4000 rpm, 30 min) and yellow-green supernatant was collected to remove un-exfoliated bulk crystals and larger-size nanosheets.[S1-S4] Subsequently, the separated supernatant was centrifuged at 10000 rpm for further 30 min, and the sediments of MoS_2 samples were isolated, respectively. Finally, the collected sediments were re-dispersed into ultrapure water for the preparation of stocking solution of liquid-phase exfoliated MoS_2 (LE-MoS_2) dispersion.

1.4. Characterization of Exfoliated MoS_2

The high-resolution transmission microscope was employed for the defects and phase identification of SL-MoS_2 nanosheets. A portion of 10 μL purified samples was dropped on an ultrathin carbon film covered Cu mesh, which was subsequently treated with an infrared baking lamp for drying. In terms of AFM and SEM records, SL-MoS_2 aqueous dispersion was dropped on a mica substrate with a fresh surface and a clean and polishing silicon chip. After the incubation for 10 min in room temperature, the aqueous dispersion on the mica and silicon substrates was removed with the blowing of nitrogen gases in case the aggregation of nanosheets with naturally drying and the simples were tested with AFM and SEM without the further treatments, respectively. The XPS measurements were conducted with the samples of SL-MoS_2 and LE-MoS_2 on silicon substrates.

2. Supporting Tables and Figures

2.1. Table S1

Table S1. Comparison of glucose electrochemical sensors based on a series of modified materials.

Materials	Techniques	Enzyme	Detection range	LOD	Modified operation	Electrode Substrate	Ref.
PdCuPt nanocrystals	Chronoamperometry	None	1-10 mM	1.29 μM	Drop-casting and drying	Glassy carbon electrode	[S5]
Polyaniline/carbon nanotubes	Chronoamperometry	None	0.05-0.3 mM	1.3 μM	Layer-by-layer assemble	Patterned Au substrate	[S6]
Nickel-niobium nanoglass	Chronoamperometry	None	0.24-4 mM	0.1 μM	Electro-deposition	Glassy electrode	[S7]
PtNi NP-GO	Chronoamperometry	None	0.5-35 mM	0.01 mM	Electro-deposition	Glassy carbon electrode	[S8]
MoS_2-Au@Pt nanohybrids	Chronoamperometry	None	10-30000 μM	1.08 μM	Drop-casting and drying	Glassy carbon electrode	[S9]
Pt nanoparticles /polyaniline hydrogel	Chronoamperometry	GOD	0.01 to 8 mM	0.7 μM	Polyreaction and electrodeposition	Platinum electrode	[S10]

Porous graphene aerogel	Chronoamperometry	GOD	1-18 mM	0.87 mM	Self-assemble	Indium tin oxide	[S11]
Graphene/platinum nanoparticles	Chronoamperometry	GOD	0-31.7 mM	0.197 mM	Rotated inkjet printing	Cylindrical flexible electrode	[S12]
PDA/ZIF-8	Chronoamperometry	GOD	1-12000 μM	0.333 μM	Drop-casting and drying	Glassy carbon electrode	[S13]
$NiFe_2$/carbon nanocomposites	Chronoamperometry	GOD	48.6-12500 μM	2.7 μM	Drop-casting and drying	Glassy carbon electrode	[S14]
Pt@BSA nanocomposites	Differential pulse voltammograms	GOD	0.05-12.05 mM	0.015 mM	Self-assemble	Au electrode	[S15]
Prussian Blue	Chronoamperometry	GOD	2-10 mM	50 μM	Printing	Screen-printed electrode	[S16]
Graphene oxide	Cyclic voltammograms	GOD	3-9 mM	0.3194 mM	Drop-casting and drying	Screen-printed electrode	[S17]
Metallic-phase MoS_2 nanosheets	Linear sweep voltammetry	GOD	0.2-100.0 mM	0.053 mM	Drop-casting and drying	Carbon fiber	This work

2.2. Table S2

Table S2. The developed strategy was compared with the blood glucose monitor for glucose measurements in samples of serum and urine, respectively.

Samples [a]	**GOD/SL-MoS_2/CPs**			**Blood glucose monitor**		
	Measured (mM)	Added (mM)	Total (mM)	Measured (mM)	Added (mM)	Total (mM)
Serum 1	5.4 ± 0.32	3.0	6.9 ± 0.22	5.2 ± 0.11	3.0	7.8 ± 0.41
Serum 2	4.3 ± 0.24	6.0	10.1 ± 0.31	4.1 ± 0.25	6.0	10.3 ± 0.36
Serum 3	5.1 ± 0.27	9.0	13.8 ± 0.15	4.8 ± 0.32	9.0	11.2 ± 0.28
Urine 1	-	3.0	3.2 ± 0.14	-	3.0	2.7 ± 0.15
Urine 2	-	6.0	5.4 ± 0.28	-	6.0	5.1 ± 0.33
Urine 3	-	9.0	8.8 ± 0.43	-	9.0	7.3 ± 0.27

[a] n=5

2.3. Figure S1

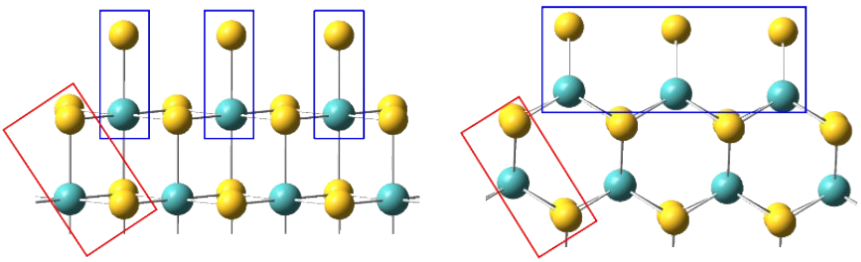

Figure S1. The initial geometry of 1T Mo_7S_{17} (Left) and 2H Mo_7S_{17} (Right). Blue balls are Mo atoms, and yellow balls are S atoms.

2.4. Figure S2

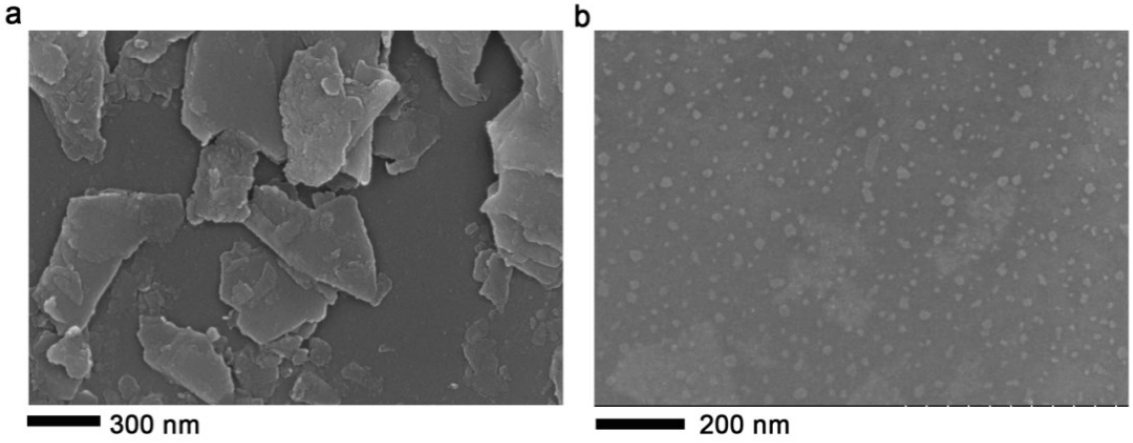

Figure S2. SEM images of bulk MoS_2 crystals before (a) and after (b) the exfoliation treatment of the SL approach. As the lack of conductivity, the sample exhibited in panel (a) was treated with gold sputtering before SEM characterizations, whereas the sample in panel (b) was directly tested without gold sputtering.

2.5. Figure S3

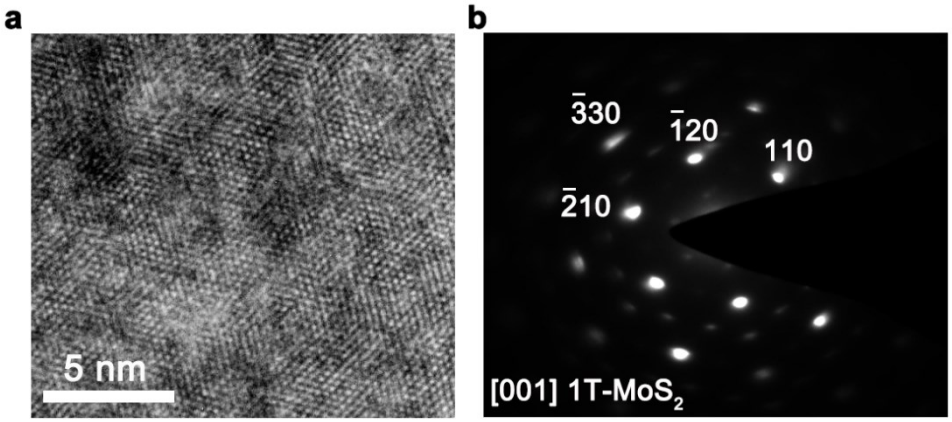

Figure S3. The HRTEM (a) and selected area electron diffraction (b) images of SL-MoS_2 indicating the metallic phase.

2.6. Figure S4

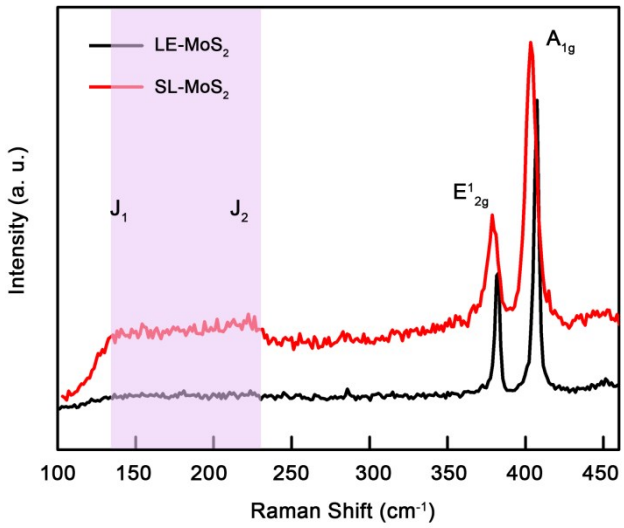

Figure S4. Raman spectra of SL-MoS_2 along with LE-MoS_2 as a comparison. The spectra are taken with an excitation wavelength of 633 nm. All spectra contain the expected MoS_2 transitions: E^1_{2g} and A_{1g}. The SL-MoS_2 has the characteristic metallic peaks (J_1 and J_2 modes).

2.7. Figure S5

The conductivities of SL-MoS_2 and LE-MoS_2 were exploited, identifying the phase characteristics. After the modification, the electrochemical impedance spectroscopy (EIS) results of SL-MoS_2 and LE-MoS_2 were recorded in comparison to the pure electrode (Fig. S5). It was found that the SL-MoS_2 modified carbon paper (SL-MoS_2/CP) exhibited lower electrochemical impedance than both pure CP and LE-MoS_2/CP. The high conductivity of SL-MoS_2/CP promoted it to be the desired electrochemical catalyst in hydrogen evolution reaction.

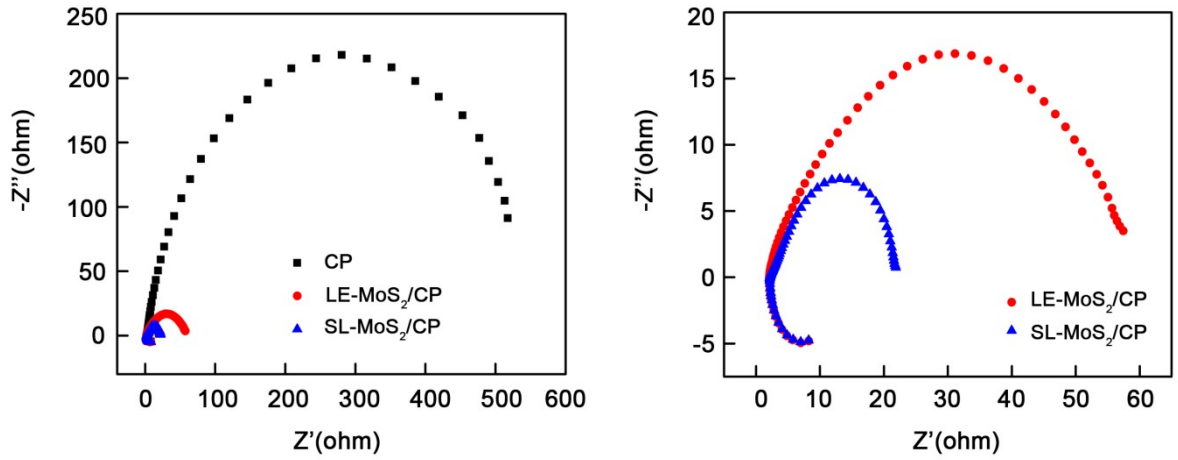

Figure S5. EIS results of pure CP, LE-MoS_2/CP, and SL-MoS_2/CP. The applied potential is -0.5 V.

2.8. Figure S6

The stability of HER performance of SL-MoS_2 was tested in comparison to that of LE-MoS_2 (Fig. S6). It was found that the even SL-MoS_2 exhibited superior electrocatalytic HER activities, the performance dropped when the testing time increased.[S18] Nevertheless, in contrast to SL-MoS_2, LE-MoS_2 performed an increasing catalytic activity when the testing time increased at a range of 0 to 1 h, which subsequently trended to be stable.

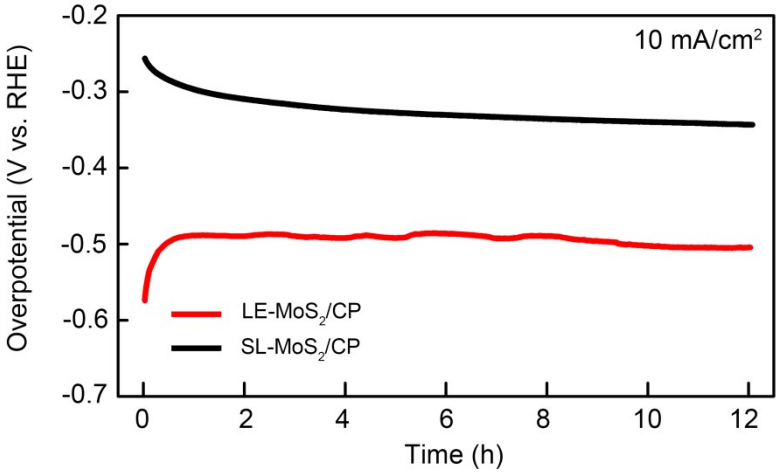

Figure S6. Over-potential tests of the LE-MoS_2/CP and SL-MoS_2/CP are measured as a function of time to maintain a current density of 10 mA/cm^2.

2.9. Figure S7

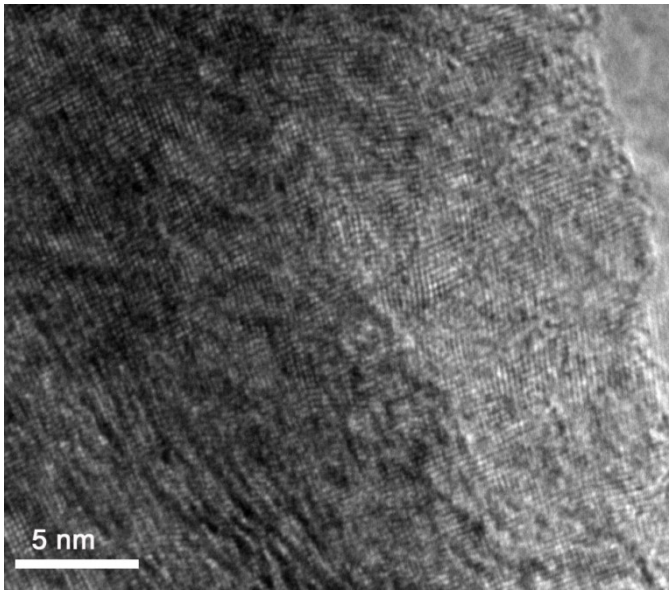

Figure S7. The TEM images of SL-MoS_2 samples collected from the SL-MoS_2/CPs after the HER stability testing.

2.10. Figure S8

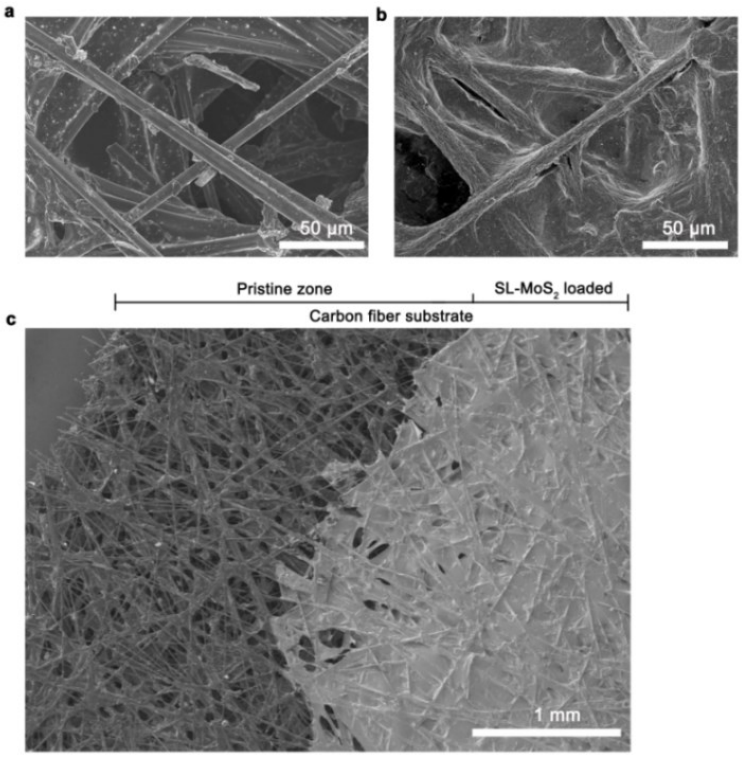

Figure S8. SEM images of the pristine CP consisting of carbon fibers (a) and SL-MoS_2 modified CPs (b and c). The samples were directly tested without gold sputtering.

2.11. Figure S9

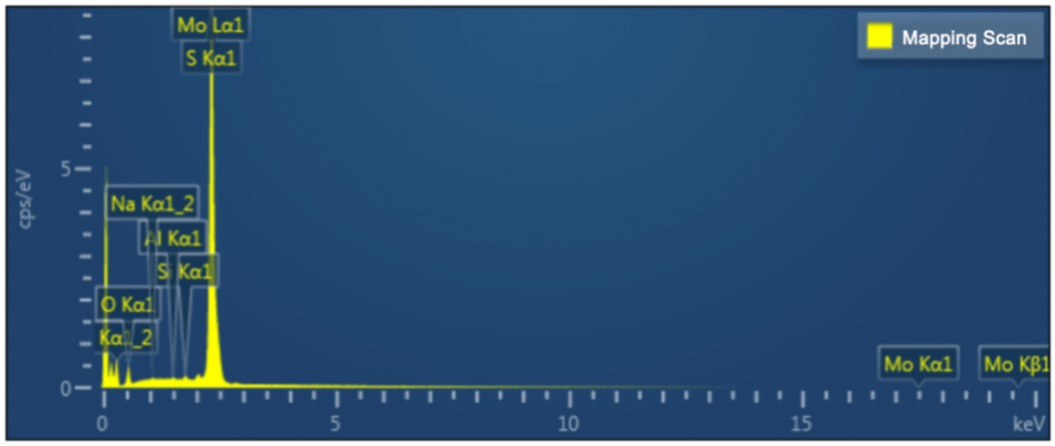

Figure S9. The EDS mapping scan result of the SL-MoS_2 modified carbon fibers.

3. Supporting References

[S1] B. L. Li, H. L. Zou, L. Lu, Y. Yang, J. L. Lei, H. Q. Luo and N. B. Li, *Adv. Funct. Mater.,* 2015, **25**, 3541-3550.

[S2] B. L. Li, M. I. Setyawati, L. Chen, J. Xie, K. Ariga, C. T. Lim, S. Garaj and D. T. Leong, *ACS Appl. Mater. Interfaces,* 2017, **9**, 15286-15296.

[S3] B. L. Li, L. Y. Peng, H. L. Zou, L. J. Li, H. Q. Luo and N. B. Li, *Small,* 2018, **14**, 1703560.

[S4] B. L. Li, H. L. Zou, J. K. Tian, G. Chen, X. H. Wang, H. Duan, X. L. Li, Y. Shi, J. R. Chen, L. J. Li, J. L. Lei, H. Q. Luo and N. B. Li, *Nano Energy,* 2019, **60**, 689-700.

[S5] S. Fu, C. Zhu, J. Song, M. Engelhard, H. Xia, D. Du and Y. Lin, *ACS Appl. Mater. Interfaces*, 2016, **8**, 22196-22200.

[S6] S. Y. Oh, S. Y. Hong, Y. R. Jeong, J. Yun, H. Park, S. W. Jin, G. Lee, J. H. Oh, H. Lee, S. S. Lee and J. S. Ha, *ACS Appl. Mater. Interfaces*, 2018, **10**, 13729-13740.

[S7] S. Bag, A. Baksi, S. H. Nandam, D. Wang, X. Ye, J. Ghosh, T. Pradeep and H. Hahn, *ACS Nano*, 2020, **14**, 5543-5552.

[S8] H. Gao, F. Xiao, C. B. Chin and H. Duan, *ACS Appl. Mater. Interfaces*, 2011, **3**, 3049-3057.

[S9] S. Su, Z. Lu, J. Li, Q. Hao, W. Liu, C. Zhu, X. Shen, J. Shi and L. Wang, *New J. Chem.*, 2018, **42**, 6750-6755.

[S10] D. Zhai, B. Liu, Y. Shi, L. Pan, Y. Wang, W. Li, R. Zhang and G. Yu, *ACS Nano*, 2013, **7**, 3540-3546.

[S11] J. Xu, K. Xu, Y. Han, D. Wang, X. Li, T. Hu, H. Yi and Z. Ni, *Analyst*, 2020, **145**, 5141-5147.

[S12] Z. Pu, J. Tu, R. Han, X. Zhang, J. Wu, C. Fang, H. Wu, X. Zhang, H. Yu and D. Li, *Lap Chip*, 2018, **18**, 3570-3577.

[S13] Y. Wang, C. Hou, Y. Zhang, F. He, M. Liu and X. Li, *J. Mater. Chem. B*, 2016, **4**, 3695-3702.

[S14] D. Xiang, L. Yin, J. Ma, E. Guo, Q. Li, Z. Li and K. Liu, *Analyst*, 2015, **140**, 644-653.

[S15] C. Hu, D. P. Yang, F. Zhu, F. Jiang, S. Shen and J. Zhang, *ACS Appl. Mater. Interfaces*, 2014, **6**, 4170-4178.

[S16] A. Martin, J. Kim, J. F. Kurniawan, J. R. Sempionatto, J. R. Moreto, G. Tang, A. S. Campbell, A. Shin, M. Y. Lee, X. Liu and J. Wang, *ACS Sens.*, 2017, **2**, 1860-1868.

[S17] M. A. Akhtar, R. Batool, A. Hayat, D. Han, S. Riaz, S. U. Khan, M. Nasir, M. H. Nawaz and L. Niu, *ACS Appl. Nano Mater.*, 2019, **2**, 1589-1596.

[S18] E. .E. Benson, H. Zhang, S. A. Schuman, S. U. Nanayakkara, N. D. Bronstein, S. Ferrere, J. L. Blackburn, E. M. Miller, *J. Am. Chem. Soc.*, 2018, **140**, 441-450.